**Rose-Hulman Institute of Technology**

**2012 ASME East Coast HPV Challenge**


# Presents

# *Carnot Cycle*

## Team Officers

**Petras Swissler**
**Ethan Rockett**
**Drew Robertson**
**Harrison Coons**

## Team Members

Simon Burns
Erin Campbell
Jeff Dovalovsky
Ben Griffith
Crystal Hurtle
Steven Keltner
Maura Lakowski
Garrett Meyer
Melissa Murray
Matt Skorina
Claire Stark
Travis Tatlock
Sam Throne
Louis Vaught
Patrick Woolfenden

**For more team information visit the team website at:**
**hpvt.rose-hulman.edu**

# 1 Abstract

During the 2011-2012 competition year, the Rose-Hulman Human Powered Vehicle Team (HPVT) designed, tested, and constructed the Carɳot Cycle. The activities of the team and the construction of the vehicle were guided by the team's mission statement:

> The purpose of the Rose-Hulman Human Powered Vehicle Team is to design a practical and commercially viable vehicle to compete in the American Society of Mechanical Engineers' (ASME) Human Powered Vehicle Challenge (HPVC) and Human Powered Race America (HPRA), and to further the goals of sustainable transportation by raising awareness for the field of human powered vehicles and implementing innovative methods, while providing a positive learning and working environment for students.

The team created a list of goals and constraints for the Carɳot Cycle based on prior observations, as well as competition rules for the ASME HPVC and HPRA events. The team used house of quality (HoQ) to improve upon previous designs. Most notably, the team developed a regenerative braking system that can also be charged from the power grid. The team also made major improvements in manufacturing, aesthetics, and practicality.

## 1.1 Constraints

The team developed a list of constraints for the 2011-2012 competition year. These constraints, shown in Table 1, are derived from three separate sources: the 2012 HPVC rules, the rules of HPRA, and the team's storage capability and budget.

*Table 1: 2012 Vehicle Constraints*

| ASME HPVC | HPRA | Rose-Hulman |
|---|---|---|
| 15 ft. (4.57 m) minimum turning radius | Rear-view mirrors | Total cost of materials and consumables of less than $10,000 |
| Braking from 15 to 0 mph (24.24 to 0 kph) in less than 20 ft. (6.10 m) | Independent and redundant braking system | The vehicle is less than 8 ft. (2.43 m) in length |
| Cargo area able to hold a gallon jug of water | | No exposed carbon fiber near rider |

## 1.2 Safety Harness

| |
|---|
| Roll bar supporting 600 lbf (2.67 kN) top load with elastic deflection less than 2 in (5.1 cm) |
| Roll bar supporting 300 lbf (1.33 kN) side load with elastic deflection less than 1.5 in (3.8 cm) |

## House of Quality

To design a vehicle that would meet customer needs, the team used a Quality Function Deployment (QFD) to re-evaluate the importance of various design considerations based on experience and new competition rules. Using the constraints listed in Section 1.1, lists of need statements and metrics were generated; these needs and metrics were then used to generate a House of Quality, available in full at rose-hulman.edu/hpv/hoq/, and shown in brief in Table B.

*Table 2: The house of quality*

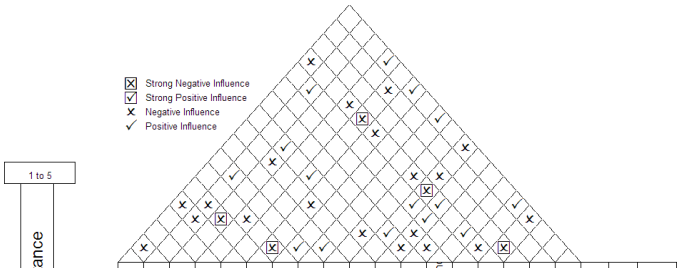


| Needs | | Roll Bar Strength | Field of View | Percent of Max. Power Produceable | Drive train efficiency | Weight | CdA | Turning Radius | Rider Satisfaction with Handling | # of Falls Out of 10 Stops & Starts | Construction Time | Number of Parts | Longest Non-Catastrophic Repair Time | Most Tools for Non-Catastrophic Repair (incl. hart | MTBF | Cost | Innovation Score | Time to Access Servicable parts | Manufacturing Tolerances | Current Competition | Planned Vehicle | Improvement Ratio |
|---|---|---|---|---|---|---|---|---|---|---|---|---|---|---|---|---|---|---|---|---|---|---|
| minimizes rider injury | 5 | 9 | 1 | | | | | 1 | 1 | 3 | | | | | | | | | | 3 | 5 | 1.67 |
| allows for riders to be aware of their surroundings | 5 | | 9 | | 1 | | | | | | | | | | | | | | | 4 | 4 | 1.00 |
| allows riders to effectively propel vehicle | 4 | | | 9 | 9 | | | | 3 | | | | | | 5 | | | | 1 | 4 | 4 | 1.00 |
| accelerates quickly | 4 | | | 9 | 9 | 9 | 3 | | 3 | 3 | | | | | | | | | 1 | 4 | 5 | 1.25 |
| has low wind resistance | 4 | | | | | | 9 | | | | | | | | | | | | 3 | 4 | 5 | 1.25 |
| handles well | 5 | | | | | | | 9 | 9 | 3 | | | | | | | | | 1 | 4 | 5 | 1.25 |
| transitions easily between stationary and moving | 3 | | | | | | | | 3 | 9 | | | | | | | 9 | | 1 | 4 | 4 | 1.00 |
| s construction is managable | 4 | | | | | | | | | | 9 | 9 | | | | | | 3 | | 2 | 4 | 2.00 |
| is quickly repairable | 4 | | | | | | | | | | | 9 | 9 | 3 | | | | 9 | 1 | 2 | 4 | 2.00 |
| is easily repairable | 4 | | | | | | | | | | | | 9 | 9 | 1 | | | 9 | 1 | 2 | 4 | 2.00 |
| is durable | 4 | 3 | | | | | | | | | | 1 | 1 | | 9 | | | | | 4 | 5 | 1.25 |
| tolerates all road and weather condtions | 4 | | | | | | 3 | | | | | | 3 | 3 | 9 | | | | | 4 | 4 | 1.00 |
| is easily transportable | 3 | | | | | 9 | 1 | | | | | | | | 3 | | | | | 4 | 4 | 1.00 |
| elided needs | 3.2 | | | | | | | | 1 | 3 | | | | | | 9 | 9 | | 12 | 3.7 | 4.2 | 1.13 |
| Absolute Importance | X | 57 | 50 | 72 | 77 | 63 | 63 | 50 | 85 | 75 | 36 | 76 | 88 | 60 | 105 | 27 | 72 | 84 | 63 | 1140 | | |
| Relative Importance | X | 13 | 14 | 8 | 5 | 10 | 10 | 14 | 3 | 7 | 16 | 6 | 2 | 12 | 1 | 17 | 8 | 4 | 10 | 150 | | |
| Current Competition | X | 116 | 180 | 70 | 70 | 45 | 0.27 | 15 | | 0 | 2800 | 110 | 30 | 5 | 2 | 15 | 3k | 14 | 60 | | | |
| Improvement Direction | X | ▲ | ▲ | ▲ | ▲ | ▼ | ▼ | ▼ | ▲ | ▼ | ▼ | ▼ | ▼ | ▼ | ▲ | ▲ | ▼ | ▲ | ▼ | | | |
| Target Value | X | 115 | 200 | 88 | 98 | 50 | 0.27 | 10 | | 0 | 2200 | 100 | 10 | 3 | 50 | 25 | 7k | 20 | 0 | | | |
| Units | X | % of spec | deg | % | % | lbf | ft^2 | ft | | falls | man-hr | parts | min | tools | hrs | pts | $ | pts | mins | | | |

Design considerations are shown in the "Needs" column of the HoQ. The metrics, shown in columns, evaluate whether those needs were met. The correlation values between needs and metrics, relative importance values, and extent of influence were assigned by consensus.

The planned vehicle and competing vehicles were compared using a scale of 1 to 5 to rate how well they met customer needs. The improvement ratio is the ratio of the planned vehicle's performance versus that of competing vehicles: ratios greater than one indicate where the team focused its efforts; rows with ratios less than one, indicating areas in which the team felt effort would be less beneficial, are omitted from the abridged HoQ. Based on these results, the team improved the manufacturability and reparability of the 2012 Carnot Cycle while maintaining a strong focus on safety and innovation.

## 2 Design

The team applied knowledge gained in past years to iterate and improve upon previous vehicles, producing a new design for the 2012 Carnot Cycle. In doing so, the team has vastly improved the performance and manufacturability of the vehicle.

## 2.1 Landing Gear

The purpose of the landing gear is to allow the rider to come to an unassisted stop during the endurance race. The landing gear system consists of three main parts: the slider, the actuation method, and the locking mechanism.

### 2.1.1 The Slider

The slider is constructed of two tightly nested square tubes, one sliding within the other. The landing gear required a minimum of 11.25 in (285.75 mm) of travel to allow it to fully retract into the fairing while still holding the vehicle upright when engaged. A small wheel on the end of the landing gear allows the rider to start with the landing gear deployed. A slot was cut out of the outer tube to allow an external actuation and return system, counter to the fully enclosed design of the 2011 Helios, which proved difficult to maintain. These features can be seen in Figure 1.

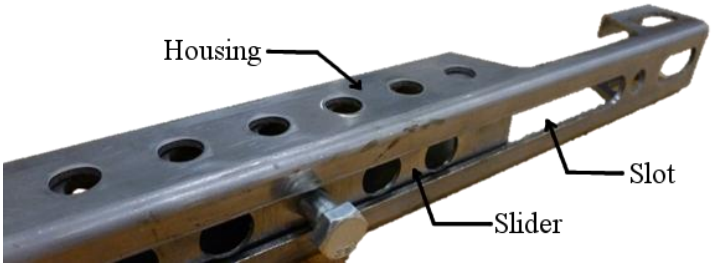


*Figure 1: Landing gear sliding mechanism.*

### 2.1.2 Actuation

Direct pull actuation was deemed unsuitable due to the large travel required. Instead, the landing gear uses a pulley system to double the actuation of the landing gear relative to the pull of the rider. Because cable was found to kink when used with pulleys, the landing gear instead uses kite string. A spring was added to ensure that the string did not lose tension and fall off the pulleys, as shown in Figure 2.


*Figure 2: The rider pulls on the actuation cable, causing a pulley to force the innermost tube to extend*

### 2.1.3 User-End Actuation

For the user-end actuation, the team considered several actuation methods for the landing gear: a pull-cable attached to the tiller (1), a lever to the side of the rider (2), and a pull-cable located over the rider's shoulder (3). All of these options are illustrated in Figure 3.

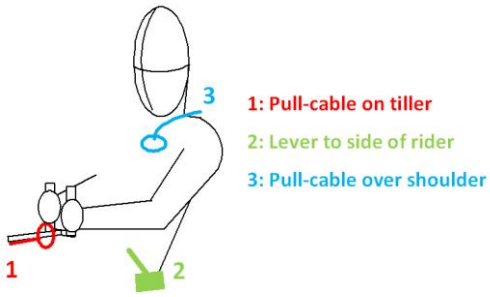


*Figure 3: Locations of Considered Actuation Mechanisms*

#### 2.1.3.1 Pull-cable on the Tiller

In this design, the rider pulls back on a ring located on the tiller to lock the landing gear in place. This was the first design considered because the team used it on the 2011 Helios. Its familiarity, as well as its relative simplicity made it an attractive option. Unfortunately, its position resulted in large amounts of resistance in the line, making it difficult to deploy or retract.

#### 2.1.3.2 Lever to the Side of the Rider

This design would involve the rider pushing a lever forward to actuate the landing gear. This design would be simple to use and would allow a locking mechanism to be easily implemented. Unfortunately, the team was unable to find a suitable location for this lever without modifying the fairing shape or interfering with the rider.

#### 2.1.3.3 Pull-Cable Over the Rider's Shoulder

This design would terminate in a ring above the rider's shoulder that is pulled to actuate the landing gear. It requires the shortest length of cable, reducing internal resistance. Riders found this to be the easiest actuation method; leading the team to implement it on the final landing gear.

### 2.1.4 Locking Mechanism

The locking mechanism was designed such that the landing gear would automatically lock in the extended position, a common request of the riders of the 2011 Helios. To accomplish this, A bungee pulls the locking mechanism to the closed position, allowing the inner tube to slide until fully extended, at which point the swing arm locks into place as shown in Figure 4. When the rider flips a shifting lever, a cable disengages the swing arm, allowing the landing gear to retract.

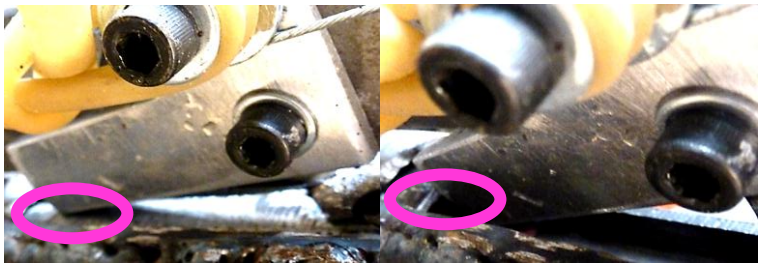

*Figure 4: The locking mechanism in action (left: unlocked, right: locked)*

Frame Design

Three general approaches exist for the vehicle frame: independent frame, unibody design, and ribbed tub monocoque.

## 2.2 2.2.1 Independent Frame

The independent frame design allows greater variation in fairing configuration, and only requires the fairing to be strong enough to protect the rider in a crash. Unfortunately, as was found in the 2011 Helios, difficulties arise when attaching the fairing to the frame; the mounting systems result in weak points. Furthermore, the complexity added by having two separate structures results in a vehicle which is heavier than other options.

### 2.2.2 Unibody

A unibody design has the fairing providing most of the structure to the vehicle. The fairing is made with a constant cross-section skin, comprised of a sheet of Nomex between layers of carbon fiber. This was employed on the 2008 Infinity. Unfortunately, the unibody design is not extremely durable, and results in large-scale delamination of the carbon fiber from the Nomex. This method also makes it difficult to implement snap fits as described in Section 2.6 and is very expensive due to the large quantities of Nomex needed for construction.

### 2.2.3 Ribbed Tub Monocoque

The ribbed tub monocoque design also uses the fairing for structure. It uses thicker ribs where strength is necessary, with thin skin in other locations, minimizing material usage and resulting in a light and very durable design. Because of these benefits, the team decided to pursue the use of a ribbed tub monocoque fairing for the Carnot. Lightweight Nomex ribs were wrapped in unidirectional carbon fiber and laid directly into the carbon fiber and Kevlar fairing. The frame layout is shown in

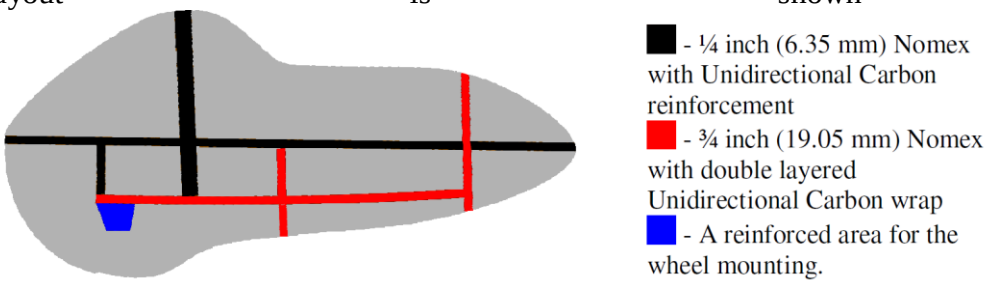


Figure 5 and its strength was verified using methods described in Section 4.2.

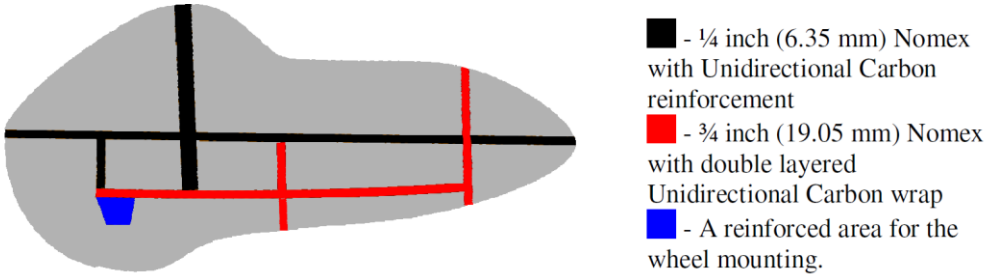

*Figure 5: Layout of ribs*

## Drive Train

On the 2011 Helios, the team used a universal joint in the mid drive to eliminate chain twisting and torque steer. That system's advantages did not justify the added complexity and mechanical losses. Therefore, the team investigated simpler drive trains for the 2012 Carnot Cycle.

### 2.3.1 Up-top Shift

In order to minimize torque steer, the team designed a drive train with shifting occurring at the mid-drive, as shown in Figure 6.

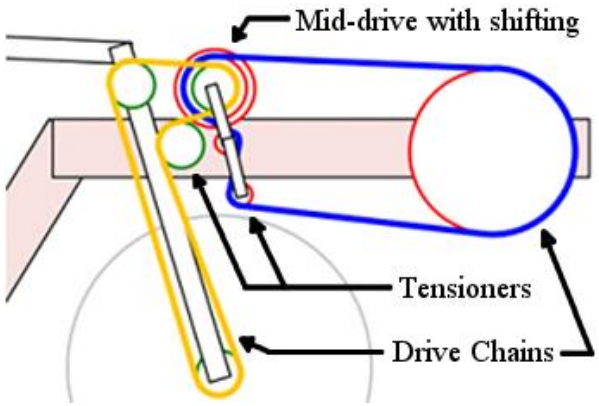


*Figure 6: Up-top shift diagram*

This design allows the point of contact between the chain and the wheel's drive sprocket to be moved closer to the steering axis, minimizing the moment arm. During prototyping, the team found that the system would be more complex than anticipated, counter to the goals of the team.

### 2.3.2 Single-chain Drive

The team explored the option of using a single chain due to expected improvements in simplicity and efficiency. The team decided that a flexing chain was not an issue, but that chain rubbing, encountered in the 2010 Ragnarök would be avoided. The chain is routed to avoid interfering with both itself and the wheel when turning. When traveling to the drive sprockets, the chain runs parallel to the head tube to diminish torque steer [1]. To increase simplicity, the drive system makes use of the inherent tensioner present in the derailleur, eliminating the need for an extra tensioner. One downside to this system is that there is no gearing at the mid-drive. To compensate, the team opted to manufacture a custom 90-tooth chain ring to achieve the optimal gearing described in Section 4.5. This design is shown in Figure 7.

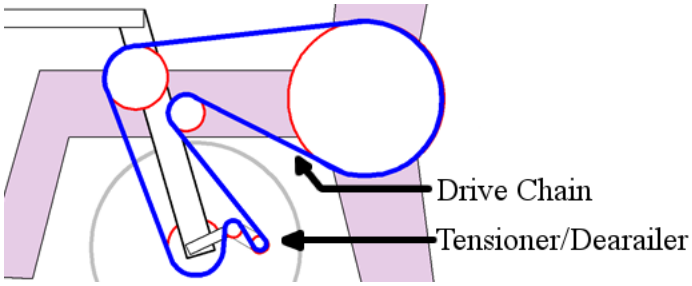


*Figure 7: A single chain is used to drive the front wheel*

Riders testing this drive train did not notice any torque steer or significant losses, so the team decided to use the single chain drive on the Carηot Cycle.

### Mold Manufacturing

2.4 The team reengineered the mold making process to increase accuracy and reduce labor requirements. In previous years, the team would craft a male mold, then used it to produce two female molds. To eliminate the inaccurate process of producing the male mold, the team decided to make use of a Computer Numerical Controlled (CNC) router, which cut the shape of each half of the female mold from foam blocks, using a SolidWorks model as a direct input.

The team cut several additional features into the mold, such as locating lines and orientation grooves, which allowed pieces, once laid up, to be placed back in their original position. The molds also made it easy to produce flanges, allowing the new seaming technique described in Section 2.5. The mold was then laid up with fiberglass, providing rigidity. After sanding, the mold was covered using packing tape.

In previous years, before each layup, three layers of wax and three layers of polyvinyl alcohol (PVA) were applied to the molds to ensure easy part removal. In total, this application process took approximately 1.5 hours per lay-up. Residual PVA would also prove difficult to remove. Eager to distance themselves from this process, the team took notice of the fact that packing tape, typically used to seal the vacuum bags, did not stick to epoxy and would leave a smooth surface.

In the fall of 2011 the team tested packing tape as the mold release for a seat mold, yielding exceptional results. With this success, the team decided employ this method on the final molds, a process taking only two hours per side. The tape performed equally well on a large scale. In total,
2.5 the result of the new approach to mold design yielded a vehicle that more accurately matched the CAD model, while saving the team an estimated 80 man-hours.

### Seaming

A new method of seaming was implemented this year using the flanges that formed around the sides of the fairing. This process greatly increased the accuracy and speed with which the seams were performed, and is illustrated in Figure 8.

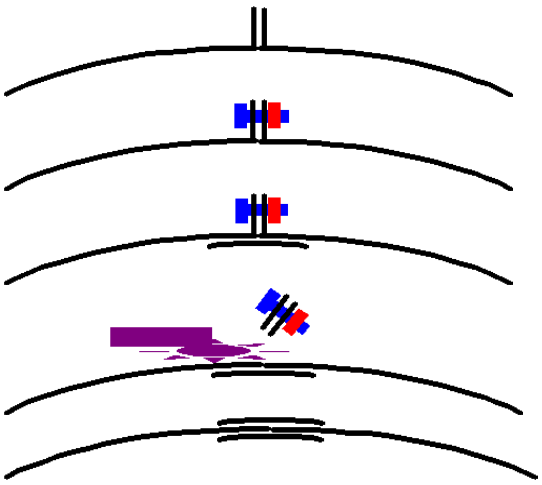

1 The two halves are aligned and butted up against one another

2 The flanges are then bolted together

3 The inside is seamed together

4 The flanges are then removed with a cutting wheel

5 The top seam is then applied

*Figure 8: Bolting the halves together allows much more accurate seaming*

### Snap Fit

2.6 A snap-fit design was implemented for the top fairing and the back hatch. Structural ribs on the removable hatches snap into groves on the main fairing, as shown in Figure 9. The rest of the fairing was laid up on top of the removable pieces with packing to guarantee accurate sizing and placement of the grooves. This ensures that the removable components stay on during competition.

2.7 *Figure 9: Matching sections of the fairing and the top hatch*

### Practicality

The Carnot Cycle is designed to be an efficient and practical form of personal transportation. Like any upright bicycle, it can be easily repaired with standard parts, and its composite fairing is corrosion resistant.

#### 2.7.1 Communication

A two-way radio was mounted in the vehicle with a microphone on the seatbelt, allowing the rider to communicate with the rest of the team. The turn signals, brake lights, and horn allow the rider to communicate with other vehicles on the track.

### 2.7.2 Fairing Openings

The Carŋot Cycle has been designed to allow the rider to put on and remove the fairing unassisted. Although this was possible in prior vehicles, it was not practical. To facilitate closing the top fairing, the top hatch was redesigned to be as small as possible. To find the minimum allowable space required for rider entry and egress, portions of an old vehicle were blocked off and riders tested different configurations. When the blocked off area covered the rider's knees, the time required to enter and exit climbed considerably. Because of this, it was determined that the fairing opening should extend just past the rider's knees.

The 2011 Helios had problems with maintenance, as there was no easy access the rear of the vehicle. This was corrected in the Carŋot Cycle with the addition of a rear hatch. This provides easy access to the rear wheel, rear disk brake, regenerative braking, landing gear, and the storage space. The fairing openings are shown in Figure 10.

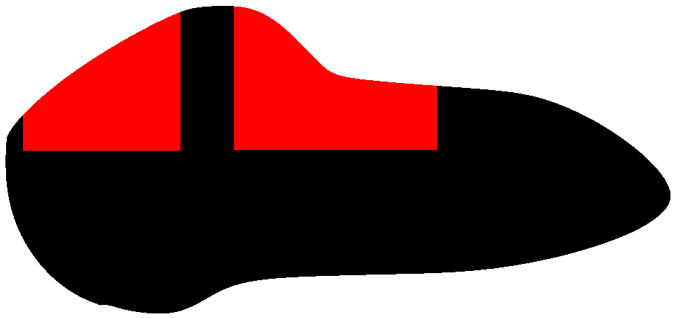

*Figure 10: Openings in the fairing highlighted in red*

### 2.7.3 Flip-Up Tiller

It was decided that the Carŋot Cycle would make use of a flip-up tiller, as previously used in the 2010 Ragnarök and the 2011 Helios. This system uses a hinge at the base of the steering tiller to fold out of the way. This makes it easier for the rider to enter and exit the vehicle, while retaining a usable tiller length.

### 2.7.4 Storage

The rules for the endurance event require that the first rider securely store and transport a gallon jug of water. The Carŋot Cycle accommodates this need by mounting a rack directly behind the rider's head capable of holding and supporting a gallon jug of water. There will be a system in place to prevent the cargo from shifting. A portion of this storage system will also serve as the headrest for the vehicle.

### 2.7.5 Electronics

Electrical systems were included to aid the rider for increased safety and utility.

#### 2.7.5.1 Lights

In the state of Indiana, all bicycles must have a white light that is visible from a distance of 500 feet (152 m) to the front and a red reflector or light must be visible from a distance of 500 feet (152 m) to the rear [2][2]. The Carŋot Cycle has two headlights placed directly in front of the mirrors. At the tail of the vehicle is an array of red LEDs. Half of the red LEDs will always be illuminated, with the other half illuminating when the brake lever is applied. To supplement these lights, reflective tape will be applied to the fairing to increase the vehicle's visibility at night. Testing showed that the lights and reflectors met the minimum requirements of Indiana.

#### 2.7.5.2 Bike Computer

A standard bicycle computer was included in the Carŋot Cycle to help riders pace themselves while riding. The display can show speed, average speed, distance, and time. The sensor was placed on the front wheel and wirelessly transmits to the main computer.

### 2.7.6 Weather Conditions

The Carŋot Cycle is most useful when the temperature inside the vehicle remains between 40°F (4°C) and 95°F (35°C). While riding in higher temperatures, the rider can remove the hatches to increase airflow through the vehicle. For most of the year, the geographical range in which the Carŋot Cycle is rideable covers most of the continental United States, from as far north as Oregon, Michigan, and Connecticut to as far south as California, Texas, and Florida [3,4][3,4][3,4][3,4][3,4][3,4]. The vehicle would also be rideable outside this region, but would be limited by extreme temperatures. In Terre Haute, Indiana—the team's location–the Carŋot Cycle would be rideable approximately 330 days per year.

When riding with all hatches on and the ventilation duct sealed, after five minutes of biking, the inside temperature would increase by at least 10°F (6°C) [5]. Rider comfort could be further increased by wearing layers of insulated clothing. The team chose to discard the average low temperatures when determining ride-ability during different seasons and locations because those temperatures generally occur overnight, an unlikely time for the vehicle to be ridden.

During precipitation, riders can use the fairing to prevent rain or snow from wetting the rider. When riding on slick roads, riders should exercise caution while turning and allow extra braking distance.

# 3 Technology Innovation

Pursuing innovation in human powered vehicles is critical to achieve viability in the consumer market. The team worked on technological innovation that would allow the Carŋot Cycle to reach out to a wider market while providing environmentally friendly transportation. When choosing a focus for technological innovation, the team quickly decided to pursue a regenerative braking system because the team felt it best met these goals.

When a rider stops from 20 mph (32.2 kph), the kinetic energy is typically lost as waste heat from the brakes. Regenerative braking allows a portion of this energy to be recaptured and

stored, with a drive motor later using it to assist the rider. The system could also be applied when going downhill, allowing the rider to summit the next hill more easily. If the field of human powered vehicles is to enter the public consciousness, the vehicles must become more than just bikes, and it is the opinion of the team this system would accomplish this goal without compromising the principles of the art.

Energy Capture

3.1 When looking at energy capture devices, the team drew inspiration from old bicycle lamps, which used dynamos to capture minute amounts of energy in order to create light. The team quickly realized that a similar system could be used to capture and convert far greater quantities of energy, eventually leading to the development of the system shown below in Figure 11.

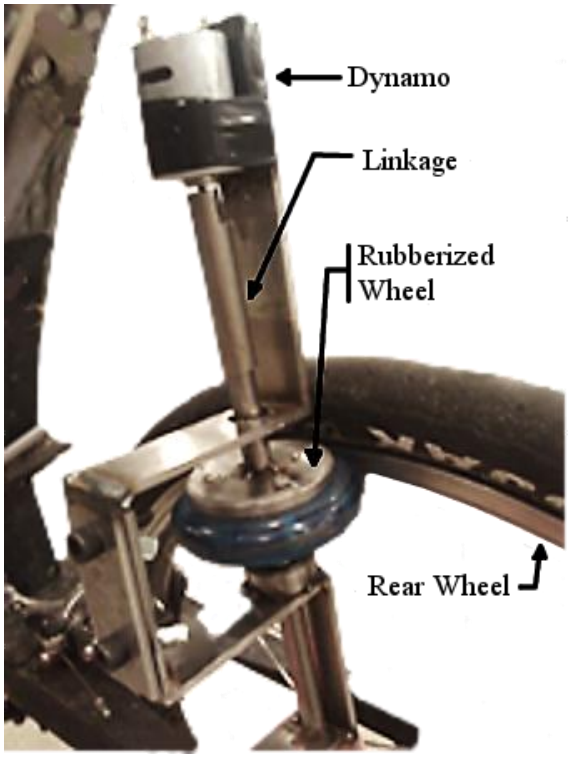


*Figure 11: The energy capture armature*

3.2 To capture the kinetic energy of the vehicle, the team constructed two armatures to act as high-power dynamos. This system straddles the rear wheel, clamping down on the rim with two rubberized wheels. When applied, these wheels spin shafts connected to two electric motors, generating an electric current. The energy extracted by this method causes the vehicle to slow. This energy is then stored in a capacitor bank

Energy Storage

Instead of using a battery, as is typical in most regenerative braking systems, the team opted instead to use electric double-layer capacitors (EDLC), also colloquially known as "supercapacitors". EDLC have a high energy density, generally hundreds to thousands of times

greater than that of traditional electrolytic capacitors. EDLC have comparable energy densities to lead acid or lithium ion batteries, but EDLC have much higher rates of charge and discharge due to their extremely low internal resistance. Because of the lack of 'memory' issues found in most rechargeable batteries, reduce the capacity of rechargeable batteries over time, the EDLCs should last the entire lifetime of the Carηot Cycle [6][6]. Furthermore, EDLCs do not contain toxic materials, making them more environmentally friendly to produce[6][6]. Supercapacitors also have advantages over batteries in safety. Unlike batteries, EDLC contain no chemicals that could explode or catch fire, even if overvolted or punctured [7,8][7,8][7,8][7,8][7,8]. The main danger with supercapacitors is their quick discharge rate, which the team will protect against by encasing the EDLCs in a faraday cage, enclosed in an electrically insulating, watertight container.

Driving

3.3 The controls for the regenerative braking system were kept simple to allow the rider to focus on the road, and intuitively placed to prevent the rider from fumbling with the controls. To use the power stored in the capacitors, the rider simply pushes a button located on the handlebars to activate a motor controller. The motor controller then sends power to the drive motor, which is connected to the rear wheel using a standard bicycle chain. To prevent this chain from creating drag during normal operation, the team has developed a bolt-on ratcheting mechanism, secured to the back wheel, which allows the chain to only affect the wheel when the motor spins faster than the wheel does.

The purpose of the drive motor is not to be the sole source of propulsion for the vehicle, but rather an assistive force for the rider. However, the team has also developed an option to turn the Carηot Cycle into an electric-human hybrid, allowing people to ride on electric power into work increasing its market appeal.

3.4

Mounting

Because the users may not want to use the regenerative braking system at all times, the system has been designed for easy removal. Because it is not integral to the vehicle, the system could be sold as an after-market add-on, extending the profits from a single Carηot Cycle.

# 4 Analysis

4.1 Analysis is a powerful tool which allows the team to converge on an optimized design without the need for multiple test cycles.

Roll Bar Numerical Analysis

To model the behavior of the roll bar under the loads specified in Section 3.C.1 of the rules, three approaches were used. First, hand calculations were performed to obtain a ballpark estimate for expected results. After this, ANSYS was used to model the composite section of the rollover protection system as an isentropic material with a constant cross-section. The Roll bar was then modeled using Siemens NX, which allows the simulation of laminate materials, ostensibly predicting deflections more accurately. These were then compared with experimental results.

#### 4.1.1 Roll Bar Hand Calculations

In 2010, the team treated the top of the roll bar as a simply supported beam [9]. This model is not entirely accurate, as there is an unknown amount of resistance to bending at the ends. Conversely, modeling it as a beam between two walls would be overly restrictive. Realizing that the best model lies somewhere between the two models, it was assumed that the total deflection would be the mean of the two deflections predicted by each model. When solved, this gives an expected deflection of 0.71 in (18 mm).

The side loading scenario cannot use this approach, as the crossbar will prevent much of the deflection that would otherwise occur, as it deflects 0.0005 in (0.0127 mm) and does not buckle. Assuming the crossbar to be perfectly rigid, all deflection at the point of loading is due to an angular deflection resulting from the couple created from the downward load and the upward reaction force from the crossbar. Therefore, the side is treated as a bar with a length equal to the height of the mock roll bar and with a torque applied at the location of the crossbar, yielding an angular deflection, $\theta$. To find the linear deflection at the point of the load, the small angle theorem is applied, simplifying the expression to (1).

$$\delta_{side} = \theta x \qquad (1)$$

Where $\delta_{side}$ is the total deflection inward, $\theta$ is the angular deflection, and x is the distance between the cross bar and the location of applied load. When solved with values measured from the roll bar, this model predicts $\delta_{side}$= 0.134 in (3.40 mm).

#### 4.1.2 Simplified ANSYS Model

A simplified model was analyzed to evaluate the performance of simple, low-precision analysis to complex, high precision analysis, in this case, with the Siemens NX simulation.

##### 4.1.2.1 Assumptions and Methodology

For the purposes of simulation, the composite section of the roll bar was treated as a constant, solid cross-section, with dimensions of the mock roll bar. Although the roll bar is essentially hollow (Nomex provides negligible strength), the roll bar was treated as a solid to prevent the possibility of the walls buckling inward, which the Nomex would preclude. Furthermore, material in the middle of a beam provides little bending strength. The material used for simulation was an adapted isentropic steel, with the values for stiffness and yield strength edited to match previously found data for unidirectional carbon fiber, 2 Msi (14 GPa) and 130 ksi (900 MPa), respectively [10]. The mounting plates were also ignored, and the roll bar was treated as if the cross bar was butted up against the composite and perfectly attached. The bar itself was modeled to manufacturer's specifications, material data was matched to a 4130 steel from MATWEB, giving a stiffness of 29.7Msi (205 GPa) and a yield strength of 63ksi (435 MPa).The roll bar was then loaded as per section 3.C.1 of the rules.

##### 4.1.2.2 Results

The simplified ANSYS model predicted that the roll bar would experience a deflection of 0.432 in (11.0 mm) when loaded vertically with 600 lbf (2670 N) at 12° towards the aft on the front

edge of the roll bar. The model also predicted that the roll bar would deflect 0.415 in (10.5 mm) when loaded from the side with 300 lbf (1330 N) horizontally at the location of the rider's shoulders, as can be seen in Figure 12.

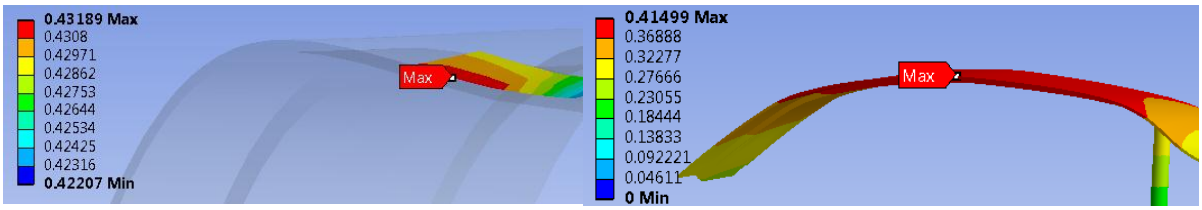


*Figure 12: Result of top loading scenario (left) and side loading scenario (right)*

### 4.1.3 Precise Siemens NX Simulation

Siemens NX is an FEA program with a strong laminate materials simulation package. Because of this, the team was eager to see what improvements this software would allow in simulation.

#### 4.1.3.1 Assumptions and Methodology

For the purposes of simulation, it was assumed that the cross-section of the roll bar is constant. Similar to the ANSYS model, the bar was treated as if it were perfectly connected to the roll bar. Loads were then applied as specified in section 3.C.1 of the rules. Material properties were obtained from CES Edupack.

#### 4.1.3.2 Results

The Siemens NX model predicted that the roll bar would experience a deflection of 0.465 in (11.8 mm) in the top loading scenario. The model also predicted that the roll bar would deflect 0.0807 in (2.05 mm) in the side loading scenario, as can be seen in Figure 13.

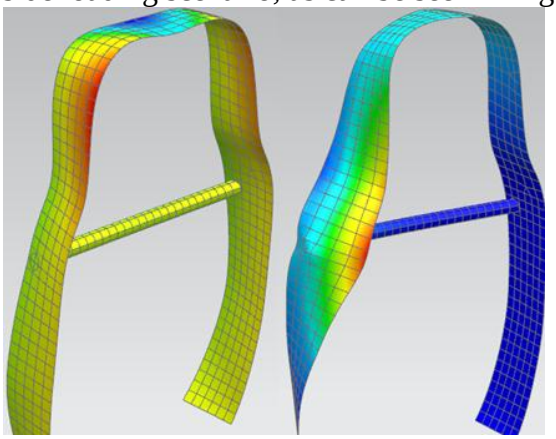

*Figure 13: Result of top loading (left) and side loading scenario (right). Both display exaggerated deflections.*

### 4.1.4 Comparison of the roll bar analyses

Table 3 summarizes these results, along with results from the testing performed in Section 5.4.

*Table 3: Summary of the Predictions of Two Different Models*

| | Top Loading | Side Loading |
|---|---|---|
| **Hand Calculations** | 0.711 in (18.1 mm) | 0.134 in (3.41 mm) |
| **Simplified ANSYS Model** | 0.432in (11.0 mm) | 0.415in (10.5 mm) |
| **Siemens NX Model** | 0.465in (11.8 mm) | 0.081in (2.06 mm) |
| **Actual Testing Results** | 0.505 in (12.8 mm) | 0.266 in (6.76 mm) |

Reassuringly, the hand calculations, though not entirely accurate, are very much in the ballpark of the FEA results, indicating that the finite element models was likely valid. This is further indicated by the closeness of the finite element models to the actual test results. The three methods performed similarly in the top loading position. However, in the side-loading condition, the Simplified ANSYS model outperformed the NX model. This is likely because the team was unable to simulate the flange on the edge where there was no Nomex. The simplified ANSYS model closely mirrored the actual testing results and it was decided that the use of a simplified model for orthotropic materials would be sufficient.

### Frame FEA

4.2 The form of the frame model was informed by two main sources: the variable geometry trainer testing performed in Section 5.2, and the stability analysis performed in Section 4.6. Although the material structure is orthotropic, it was found in Section 4.1.4 that isotropic models could accurately represent reality within reasonable tolerances. In order to verify that using an isotropic model was accurate, the team compared the two methods by modeling and analyzing a simple beam in torsion and bending, the predominant types of loading in the frame. The members were analyzed using isotropic analysis in ANSYS, as well as orthotropic analysis in Siemens NX. These test simulations showed that the simple isotropic model agreed with the orthotropic model to within about 10% accuracy. Therefore, an isotropic model was used for simplicity.

Two primary loads were applied to the frame to simulate a worst-case scenario: a 200 lbf (890 N) force simulating a person sitting in the vehicle, and a 100lbf (445 N) pedaling load. These loads were given an impact loading factor of three, as was used in the design of the 2011 Helios [5]. An acceptable frame could withstand these loads with a factor of safety in stress of at least two. Stress visualization for this case is found in Figure 14.

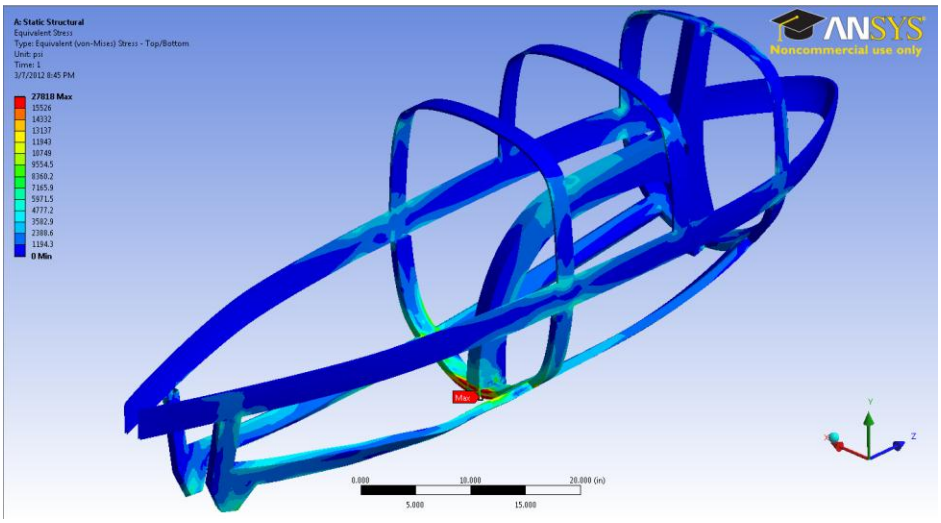


*Figure 14: Stress Visualization of Frame Under a Load*

The maximum stress in the model occurs at the transition between the sub-frame and the back rib with a stress of 27.82 ksi (191.8 MPa). When compared to the strength of unidirectional carbon fiber, this gives a factor of safety of 5.4, showing that even under impact loading the vehicle's frame will remain undamaged. Additionally, the intersections of the ribs were the areas of highest stress. These areas have additional reinforcement due to the overlaps from seaming (Section 2.5) which were not modeled.

## 4.3 Wind Conditions

The combination of wind and the motion of the vehicle combine to produce an apparent wind angle, or angle of attack. Consequently, a faster-moving vehicle will be less affected by cross-wind. The weighted probabilities of each wind angle were calculated using a MATLAB program as described in the 2010 and 2011 Rose-Hulman design reports, using the mean wind speeds for Grove City, PA and Salt Lake City, UT. Based on National Weather Service data, these wind speeds were found to be 10.5 mph (16.9 kph) and 9.6 mph (15.4 kph) [11][11].

The resulting weighted cumulative distribution of the apparent wind angle indicates that 82.5% of the expected winds occur at an apparent angle of less than 20°, which corresponds to a 16.5 mph (26.6 kph) cross wind at 45.5 mph (73.0 kph). Based on this analysis, fairing aerodynamic simulations were conducted as described in Section 4.4.

## 4.4 Computational Fluid Dynamics

The team used a computational fluid dynamics (CFD) model to simulate the air flow around the fairing in order to minimize aerodynamic drag. ANSYS FLUENT was used to test both headwind and crosswind conditions. Tests were conducted near the vehicle's desired top speed of 45.5 mph (73.0 kph) with crosswinds of 0 mph (0 kph), 8 mph (12.9 kph) and 16.5mph (26.6 kph). These results were then multiplied by the probability of encountering them (based on the results of Section 4.3) of 0.3, 0.4, and 0.3 respectively. The sum of these values was minimized to find the most aerodynamic fairing for the conditions the vehicle would encounter.

To create a more comprehensive model, the ground and its velocity with respect to the vehicle were included. The wheels were also modeled as rotating rather than static, and turbulence was modeled using the Spalart-Allmaras method which is adept at handling medium-speed airfoils and the transition from laminar to turbulent airflow.

The initial model was created to encompass a set of cross sections determined by the motion capture, described in Section 5.1, and the team's experience. Various CFD visualization tools, including surface pressure plots and particle flow trajectories, were used to identify areas where each model could be improved. The fairing model was then optimized for its aerodynamic characteristics, retested and reanalyzed.

After numerous iterations, the team reached the final design for the Carηot Cycle. The Carηot Cycle is slightly wider than the 2011 Helios, particularly at the shoulders to avoid cramped conditions inhibiting rider comfort and to ensure that a wider range of consumers would fit in the vehicle, broadening the potential market. This year, shipping and mold-making constraints limited the length of the vehicle to less than 8 feet. Despite the increase in cross section, the drag force was decreased due to the back fin and a rounder cross section. Using the drag force and side force values calculated in each of the FLUENT simulations, the coefficient of drag times area, $C_dA$, assuming no crosswind was found using Equation (2).

$$F_d = C_d A \cdot \rho \frac{V^2}{2} \qquad (2)$$

Table 4 shows the results of the CFD analysis. The side force is the perpendicular component acting to push the vehicle over, and is vital to handling in inclement weather. At 20 mph, each vehicle experiences a forward force, as noted by the (-), analogous to a sailboat tacking into the wind.

*Table 4: Designs and Performances*

| | Crosswind Speed mph (kph) | | | Weighted Average lbf (N) | Side Force lbf (N) | $C_dA$ ft$^2$ (m$^2$) |
|---|---|---|---|---|---|---|
| | 0 (0) | 8 (12.9) | 16.5 (26.6) | | | |
| | Drag Force lbf (N) | | | | | |
| **2011 Helios** | 3.39 (15.1) | 2.45 (10.9) | -0.64 (-2.84) | 1.81 (8.03) | 51.1 (226.9) | 0.641 (0.0596) |
| **Initial Model** | 3.26 (14.5) | 2.31 (10.3) | -0.48 (-2.13) | 1.73 (7.69) | 56.3 (250) | 0.617 (0.0573) |
| **Carηot Cycle** | 3.16 (14.0) | 1.96 (8.70) | -1.73 (-7.68) | 1.21 (5.40) | 54.4 (241.5) | 0.597 (0.0554) |

4.5 Gearing

The gear ratio was determined by the ability to reach 45 mph (72 km/h) while maintaining a cadence between 80 rpm and 110 rpm over a range of 10 mph (16 km/h) to 40 mph (64 km/h). The team has only attained speeds of 45 miles per hour during sprint races, when a higher cadence is acceptable. Therefore, the gear ratio was designed to maintain a reasonable cadence during the endurance event. Figure 15 displays the speed as a function of pedal cadence for different gear ratios.

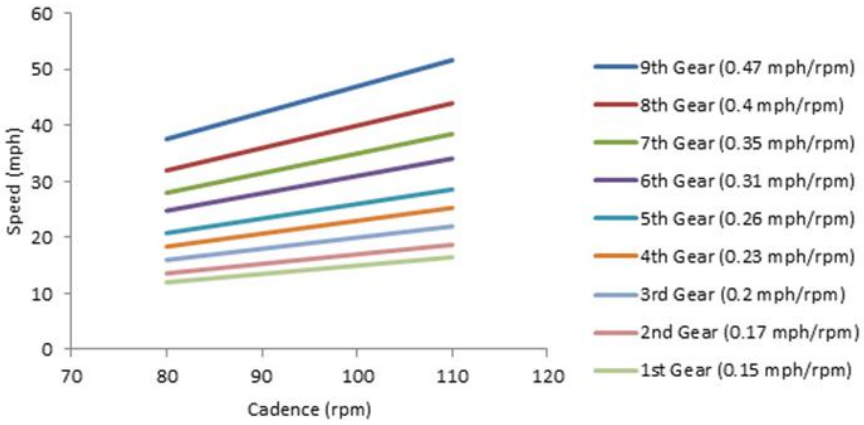


*Figure 15: Available cadence to speed ratios*

To achieve the desired gear ratios, the Carŋot Cycle uses a custom-made 90-tooth front chain ring and a cassette at the hub with a range of an 11 tooth gear to a 34 tooth gear. These large chain rings could be easily mass-produced, minimizing cost to the consumer.

### 4.6 Stability

The wheel base of the Carŋot Cycle was derived from the 2011 Helios and 2010 Ragnarök and the rider position was determined by the variable geometry trainer testing. The vehicle's steering geometry was designed using a MATLAB program based on Dr. William Patterson's "The Lords of the Chainring." To increase manufacturability, the fork was designed with no offset. Low speed steering input force and steering sensitivity were reduced by finding the optimal head tube angle with the aid of the MATLAB program. To verify the geometry called for by the program, the team built a steel prototype with the same geometry as the final vehicle. The vehicle excelled at both low and high speed handling.

### 4.7 Cost

The team believes that a single mold could be used to produce 20 Carŋot Cycles before a new one would have to be made, but that the release agent would have to be replaced every two vehicles. Using the costs from the current competition year for vehicle consumables and mold costs (found in Appendix A), the total equivalent cost of producing a Carŋot Cycle would be $2,150 per vehicle. The team estimates that it would take skilled workers approximately 75 man hours to construct the vehicle. Assuming each worker earned $25 per hour, the total equivalent cost per vehicle would be $4020, meaning that the vehicle could be sold in the $6500 range. The team believes that if marketed as human-electric hybrid, this price would be highly palatable for the general public. Aftermarket options could extend profitability.

# 5 Testing

Testing is often necessary either due to a system being too difficult or uncertain to model, or to verify analysis.

### Motion Capture

To ensure reasonable clearances between the rider and the fairing, data was collected from four test subjects riding a customizable recumbent trainer. Three Qualisys Track Manager IR cameras recorded the x-y-z coordinates of reflective balls placed on each rider's joints, as shown in Figure 16. Although similar tests were performed in the design of the 2011 Helios, increased accuracy was achieved by repeating motion capture with the new seat position. Because pedaling motion differed with speed, each rider was recorded as they started to pedal, maintained a comfortable long-distance pace, and then sprinted [9].

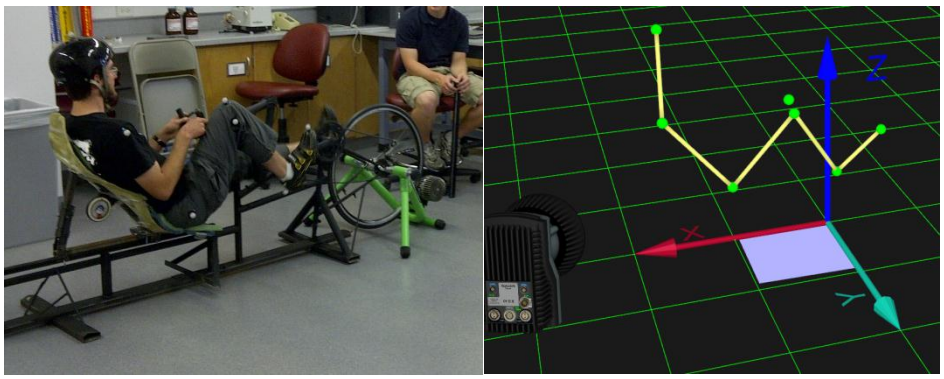


*Figure 16: Motion Capture Testing (left) and Qualisys Track Manager Interpretation (right)*

A MATLAB program used these points to determine the volume riders used while pedaling. After interpreting the points as joints, the program uses a convex hull algorithm to find the smallest convex polyhedron encompassing these points, resulting in the shape in Figure 17.

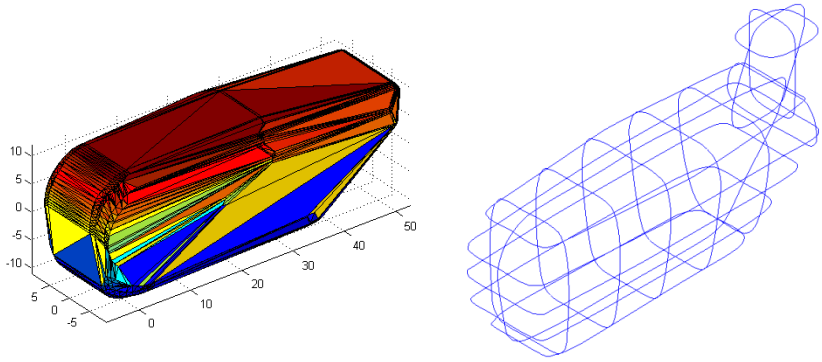


*Figure 17: Convex Hull of Rider Space and Wire-Frame Model*

Cross sections of the polyhedron were then generated and imported into SolidWorks.

### Power Output Testing

The most ergonomic rider position was determined through a series of tests. Because previous results revealed that the power output of different riders followed similar trends, the team elected to conduct testing using a single rider while considering more variables. One-minute spinning-start trials were conducted on a variable geometry trainer, with power measured using a power-

tap hub and recorded on a Garmin cyclocomputer. Immediately after each trial, the subject rated the comfort of the position. Geometry was defined as shown in Figure 18.

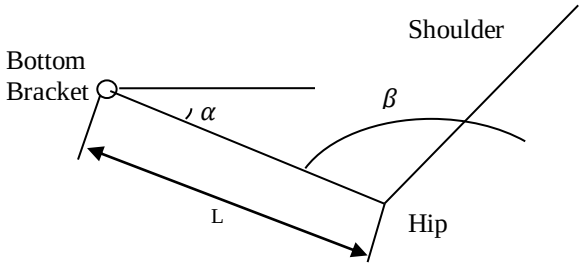


*Figure 18: Variable Geometry Trainer*

An initial half-factorial screening test showed that the angle α, shown in Figure 18, did not significantly impact the power output of the rider. A full factorial test conducted on the remaining three variables, $\beta$, $L$ and crank length showed no significant interactions, allowing each to be tested separately. It was found that leg extension, L, affected rider comfort but had negligible effect on power output. The team also found that a β of 121° resulted in the highest power output. The tests revealed that 155 mm cranks resulted in a higher power output but lower rider satisfaction compared to 175 mm cranks. This contradicts previous results by the team, but is not unreasonable considering that many riders get best results from 165mm cranks [12][12].

## 5.3 Regenerative Braking

The team conducted two tests to validate the design of the regenerative braking system: energy capture from the braking system with subsequent energy storage, and energy discharge through the drive motor. Tests were conducted under ideal conditions.

### 5.3.1 Energy Capture and Storage

When a rider slows from 20 miles per hour to a full stop, the dynamos will see a rotary input ranging from 2500 rpm to 0 rpm. Although the rotation would slow continuously, dynamos were run at the maximum of this range to simplify testing. The output voltage was measured using a multimeter. Figure 19 shows the data for the voltage across and energy stored by the EDLC.

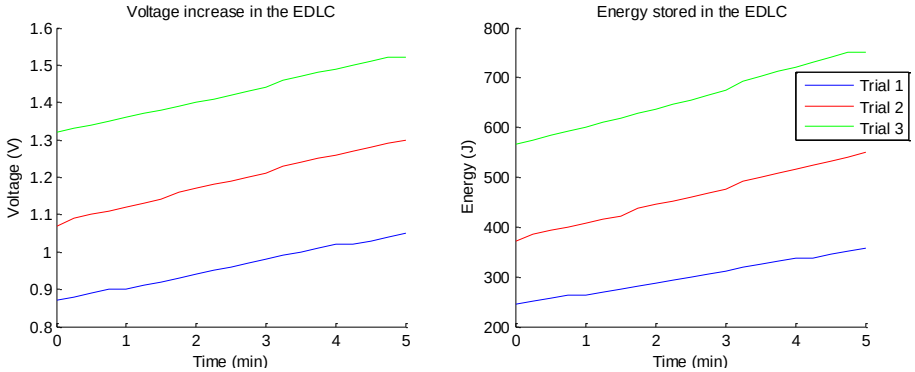


*Figure 19: Data for the charging of an EDLC over the course of five minutes. 3 subsequent trials are run, hence each trial beginning where the other left off.*

As evidenced by the data, over the five minute testing period the overall voltage of the EDLC bank increased by an average of 0.203 V resulting in an average energy increase of 158 J. This test utilized a single charging dynamo, and the results would increase with a greater number of dynamos utilized in parallel by generating more current at the same voltage.

### 5.3.2 Energy Discharge Through a Drive Motor

The 650 F EDLC bank is charged to 9.5V, storing 29.3 kJ. The bank is then discharged through the drive motor until the voltage of the EDLC bank drops below the operating voltage of the motor (found to be 6.8V). To control the motor, a 30A relay was employed to control the circuit due to high expected currents. A data acquisition system monitored the EDLC bank as well as the motor. This data is plotted in Figure 20.

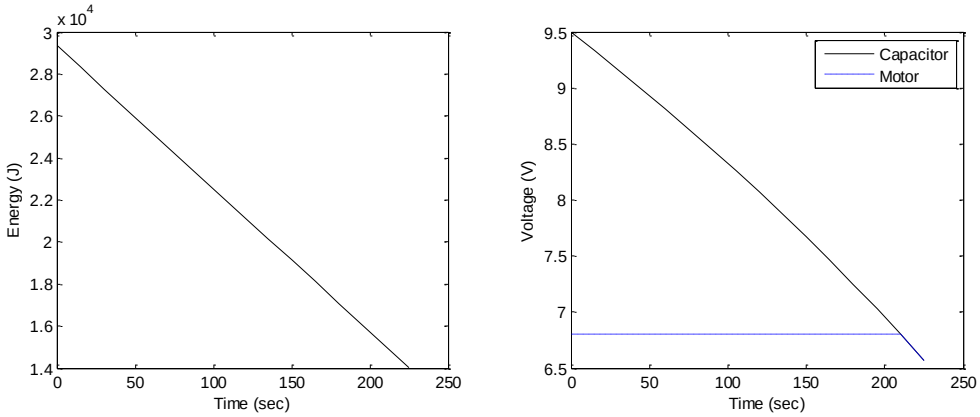


*Figure 20:Discharge test results*

A typical rider will output 250W during the competition; if used to supplement the power of the rider, the motor power output of 68W results in a 27% increase in power to the wheels [13]. These results confirm the viability of the regenerative braking system for the consumer market.

## 5.4 Roll Bar

The rollover protection system used in the Carηot Cycle is a composite roll bar integrated into the fairing. To confirm the strength of this system, the team manufactured a mock roll bar with the exact geometry and composition of the final roll bar. Although previously analyzed in Section 4.1, physical testing is needed to confirm this analysis.

To comply with ASME HPVC rules, a roll bar must, without permanent damage, withstand a 600 lbf (2670 N) load, applied to the top front edge, angled backwards at 12° from vertical with a maximum deflection of 2 in (5.1 cm). It must also withstand a load of 300 lbf (1330 N) applied horizontally at the shoulders with a maximum deflection of 1.5 in (3.8 cm). In the top loading scenario, the roll bar deflected a maximum of 0.505 in (1.27 cm). When loaded from the side, a maximum deflection of 0.266 in (0.676 cm) was recorded. Neither case exhibited signs of permanent damage, meaning that the rollover protection system met all specifications for the ASME HPVC.

The failure load of the roll bar was determined by using the tensile tester to produce a 2 in (5.08 cm) deflection. This resulted in a maximum supported load of 1305 lbf (5805 N). This value is slightly less than the maximum 1390 $lb_f$ (6.18 kN) supported by the roll bar of the 2011 Helios and the 1430 $lb_f$ (6.34 kN) of the 2010 Ragnarök [5,9]. However, the deflection experienced by the current roll bar at maximum force was less than that experienced by previous roll bars, possibly due to the use of a cross-bar.

### Carbon Fiber Structural Members

Three different layup techniques were used to lay-up carbon fiber tubes to determine the manufacturability and strength of each for use in the subframe. The samples were made of polystyrene foam cores wrapped in carbon fiber. The first sample had a rectangular cross section and was wrapped with two layers of 11-ozsy carbon fiber weave with unidirectional carbon fiber on the top and bottom. The second sample had notches on top and bottom and was wrapped with unidirectional carbon fiber at 45 degree angles. The third sample had slots on the sides and was wrapped identically to sample 2. These samples are depicted in Figure 21.

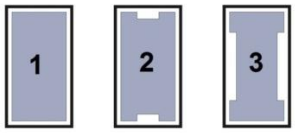


*Figure 21: Carbon Tube Designs*

When put into a vacuum, the carbon fiber was pulled down into the channels of samples 2 and 3 and removed many of the wrinkles that were found in the first sample. However, sample 1 was easier to fabricate. Tensile testing showed that sample 3 was the strongest, as seen in Figure 22.

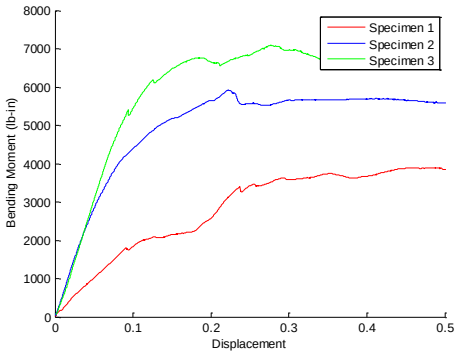


*Figure 22: Data for specimen tests of carbon tube designs.*

However, it was found that samples 2 and 3 weighed more per unit length than sample 1, which still possessed acceptable strength. Because of this, as well as its increased manufacturability, method 1 was chosen as the basis for the structure of the subframe.

### Resin Transfer Molding

The team tested the feasibility of using resin transfer molding (RTM) to manufacture the Carnot Cycle. Unlike wet lay-ups, with RTM, materials are placed into the mold dry. A vacuum then draws resin into the material. This method eliminates time constraints due to epoxy gel time, reducing human error. Figure 23 depicts this technique.

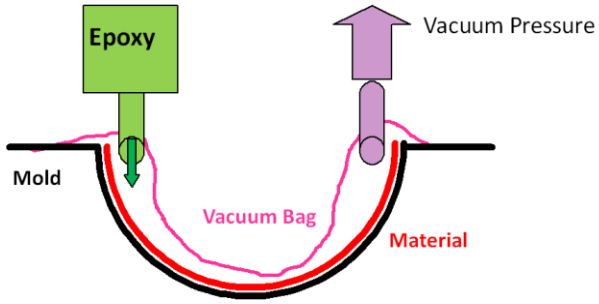


*Figure 23: Diagram depicting an RTM system*

To perform feasibility testing on RTM, a small mold with tight geometries was used with an RTM system and low-viscosity epoxy. Unfortunately, this RTM system could not saturate the material due to low flow rates. Furthermore, using RTM would fill the Nomex honeycomb, increasing the weight of the vehicle. Consequently, the team decided not to pursue RTM.

## Skid Testing

When sliding, the surface will undergo significant wear. Because of this, the team decided to test the use of automotive trim to minimize contact with the ground and shorten the distance of a slide. To do this, the team placed strips of automotive trim on the right side of the 2009 Mark IV, leaving the left side for a control test. The strips were placed such that it would almost entirely eliminate contact between the fairing and the pavement. The team then accelerated the vehicle to approximately 20 mph (32 kph) before initiating a crash.

During testing, it was clear that the sliding distance with the automotive trim was far shorter than that without, with an approximate reduction of 33%. This increases safety, as the Carnot Cycle will be less likely to slide into barriers. Because of this as well as the increased wear resistance, the team decided to use automotive trim on the Carnot Cycle.

### Visibility

With safety being the primary concern of the team, superior visibility for the rider is imperative. To verify that the rider will be aware of his or her surroundings, a test was performed to ensure proper visibility. A mock-up of the major sight impediments was constructed on the prototype. Three separate team members took turns reporting the limits of their visibility. The total visibility was then calculated using the average positions of these limits.

The team found that the rider is given 180 degrees of clear line of sight. Furthermore, the side mirrors increased the visibility by another 90 degrees. As shown in Figure 24, the rider can see 75% of road surface within 50 ft (15.2m) of the center of the vehicle.

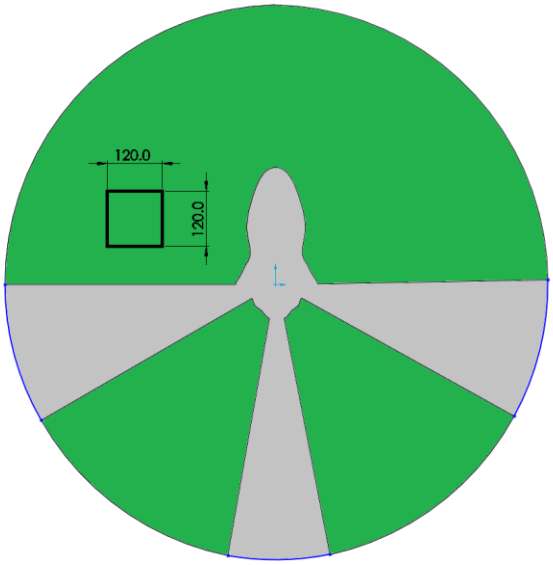


*Figure 24: Visibility in the immediate vicinity of the vehicle, units in inches*

This visibility allows the rider to confidently navigate roadways and obstacles, greatly reducing the likelihood of a crash.

# 6 Safety

In addition to design decisions detailed in Section 2, the team undertook several other measures to ensure the safety of its riders.

## 6.1 Roll Bar

When designing the roll bar, the team wanted to minimize weight while increasing the safety of the rider. To accomplish this, the team removed several layers of carbon fiber, saving weight, and replaced them with a crossbar, to stiffen the side. The exact lay-up configuration is shown in Figure 25.


*Figure 25: Roll bar lay-up materials*

A composite roll bar is included in the Carɳot Cycle to ensure the safety of the rider. It is positioned to provide protection without obstructing the rider's field of view. The roll bar exceeds the set requirements for it, as described in Section 4.1 and 5.4, and weighs less than in previous years.

### Materials

To ensure the safety of the rider, the team decided to line the inside of the vehicle with Kevlar, as it has been shown to significantly decrease the prevalence and sharpness of carbon shards in the event of a fracture [9]. The team also used a trim on the edges of the main and top fairing to eliminate sharp edges and prevent delamination.

6.2

### Windshield

When designing the fairing, the team ensured that a 2D curve was present in the head bubble area. Because of this, the windshield is much easier and faster to manufacture (heat forming is not required) as the polycarbonate, which is used for its impact resistance, can be easily bent into shape. To attach the windshield, 0.125 in (3.175 mm) Nomex was laid into the top hatch, and was later chiseled out, allowing the polycarbonate to take its place. Through this method, the windshield sits very securely, allowing it to protect the rider, even in the event of a crash. As mentioned previously in Section 5.8, it was found that the windshield and mirrors gave a total of 270 degrees of visibility, exceeding the requirements.

6.3

### Seatbelt

6.4

The seatbelt on the Carŋot Cycle is a three-point harness identical to that used on the 2011 Helios, and was selected over a four-point harness to allow easy entrance and egress. The attachment method is identical to the Helios as well: the seat belt is secured against the roll bar via a steel plate, which is held in place with five rivets. Based on previous testing, the seat belt will hold a total of 1650 lbf (7335 N) before failure [10], meeting the specifications set forth in the rules.

6.5

### Safety Features on Regenerative Braking

The drive motor can draw large amperages, up to 20A, which is more than the wiring allows. A current regulator is used to prevent this from occurring. This reduces the risk of a short causing a large current spike. To help prevent shorts, all electrical connections are covered. These safety measures, along with measures described in Section 5.3, will ensure the safety of the rider.

6.6

### Shoulder Protection

Included under the edges of the top hatch are a pair of skid zones, as shown in Figure 26, which protect the rider from injury during crashes when the top is absent. It protects riders by keeping shoulders and elbows from contacting the ground and getting road-rash. Although this system does slow entrance and egress, the protection provided is very beneficial to riders.

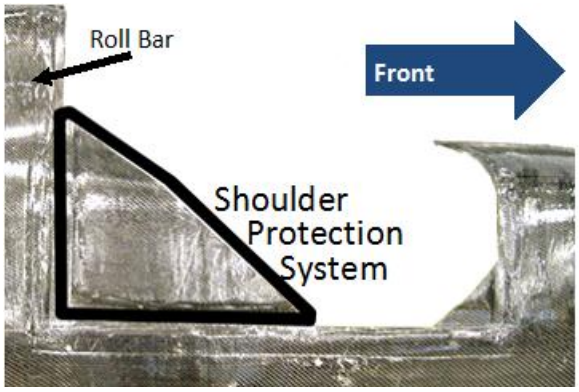


*Figure 26: Shoulder protection system*

### Helmet

6.7 Helmets are one of the many safety features employed by the team. The typical bicycle helmet is designed to crush to reduce the rate at which the skull and brain are accelerated. Recent studies indicate that "helmets provide a 63 – 88% reduction in the risk of head, brain and severe brain injury for all ages of bicyclists" [14]. Thus, the vehicle was designed to accommodate a helmet.

### Maintenance

6.8 The team recommends that users of the Carŋot Cycle perform at least one complete teardown every year to inspect all parts of the vehicle for signs of wear and corrosion. Also recommended are seasonal inspections of the braking, drive, and landing gear systems to ensure performance in all weather conditions.

6.9 ### Safety of Manufacturability

To ensure the safety of manufacturing the vehicle, the team employed a three-pronged approach. First, all members were trained in the safe use of power tools, and were not permitted to work alone when using power tools. The team also took great effort to ensure a clean workspace. Second, all members were required to use the proper personal protective equipment (PPE) when engaging in team activities. Examples of PPE include the use of respirators when sanding and wearing safety glasses at all times.

Finally, several decisions were made to increase the safety with which the Carŋot Cycle could be assembled. The most major of these decisions was to use epoxy resin instead of the cheaper, but toxic polyester resin. Furthermore, sharp edges of the flanges present on the fairing components were immediately trimmed off to prevent a member from cutting themselves. Also important was the continual effort to allow members to work on the vehicle in an ergonomic stance. Although less important for the production of the competition vehicle, if mass-produced, this could greatly help worker health over time.

A new silencer was also developed for the Venturi nozzle the team uses to draw a vacuum. With a silencer ordered online, noise from the Venturi was significantly reduced, but team members still had to elevate their voices to communicate with others in the immediate area. Realizing that

this could cause safety issues (both through the inability to communicate dangers to others and long-term hearing loss) the team developed a higher quality silencer for use with the Venturi nozzle. This was accomplished by stuffing a small amount of batting into a medium diameter pipe with hose fittings at either end. This reduced the noise to much lower levels, but still made it difficult to communicate with others on the opposite end of the workspace. To further enhance the silencer, a cone made of soft paper was and mounted inside a plastic cup, which was then attached to the end of the pipe. This resulted in the Venturi nozzle being almost entirely silent, thus creating a safer work environment.

# 7 Aesthetics

An important factor in a client's decision to purchase a product is the appearance. For this reason the team has done as much as it could to improve the aesthetic appeal both in the near-term, as well through the course of the life of the vehicle.

To ensure that the Carɳot Cycle is attractive before use, several methods are employed. First, the snap fits described in Section 2.6 ensure that removable fairing components fit snugly without unattractive gaps. Attention is also given to the paint scheme, which is not only designed to appear speedy, but also serves to mask the seams, which could otherwise appear unattractive. The interior is also painted to allow the vehicle to appear attractive regardless of fairing configuration. Care is given to internal components to appear clean and professional, and waterproof paint is used to allow for easy cleaning of the vehicle.

When considering the long-term appearance of the vehicle, the team realized that the crashes inevitably undergone by the Carɳot Cycle should minimally impact the durability of the vehicle. To accomplish this, the vehicle uses the automotive trim described in Section 5.7. The team has also switched from using Bondo as a filler material for fairing imperfections due to its unattractive salmon color. Instead, the team has switched to using chopped fiber, which is made by cutting up scrap pieces of carbon fiber and separating individual fibers, then mixing with epoxy to give a fuzzy filler material. Chopped fiber appears very similar to laid up carbon fiber, and will degrade more gracefully than does Bondo.

**Appendix A: Costs**

## Consumables Per Mold

| | |
|---|---|
| Fiberglass | $ 92.40 |
| Epoxy | $ 110.00 |
| Foam | $ 700.00 |
| Release Coating | $ 13.20 |
| Breather Cloth | $ 30.00 |
| Peel Ply | $ 70.80 |
| Plastic Sheet | $ 12.80 |
| Subtotal | $ 1,029.20 |

## Regenerative Braking

| | |
|---|---|
| Wheels | $ 2.50 |
| Sprockets | $ 20.00 |
| Chain | $ 10.00 |
| Small motors | $ 8.00 |
| Drive motor | $ 30.00 |
| Capacitors | $ 146.67 |
| Subtotal | $ 217.17 |

## Electronics

| | |
|---|---|
| Wires | $ 5.00 |
| White LEDs | $ 20.00 |
| Red LEDs | $ 15.00 |
| Bike Computer | $ 40.00 |
| Subtotal | $ 80.00 |

| | |
|---|---|
| Total Per Mold | $ 1,029.20 |
| Total Per Bike | $ 1,743.23 |
| Regenerative Breaking | $ 217.17 |
| Electronics | $ 80.00 |
| Total | $ 3,069.60 |

## Consumables Per Bike

### Fairing

| | |
|---|---|
| 11oz Weave | $ 315.00 |
| Unidirectional | $ 119.00 |
| Kevlar | $ 63.00 |
| Epoxy | $ 82.50 |
| Plexiglass | $ 7.00 |
| 1/4 in Nomex | $ 36.13 |
| 3/4 in Nomex | $ 30.10 |
| Roll Bar Bar | $ 7.50 |
| Subtotal | $ 660.23 |

### Subframe

| | |
|---|---|
| Foam | $ 2.70 |
| 11oz Weave | $ 35.00 |
| Unidirectional | $ 21.00 |
| Head tube | $ 37.00 |
| Bottom Bracket | $ 26.00 |
| Steel Plates | $ 8.00 |
| Subtotal | $ 129.70 |

### Bagging Materials

| | |
|---|---|
| Breather Cloth | $ 50.00 |
| Peel Ply | $ 76.70 |
| Plastic Sheet | $ 25.60 |
| Subtotal | $ 152.30 |

### Other Components

| | |
|---|---|
| Seat Belt | $ 44.00 |
| Landing Gear | $ 18.00 |
| Wheels | $ 231.00 |
| Fork | $ 30.00 |
| Shifters | $ 80.00 |
| Brakes | $ 89.00 |
| Drivetrain | $ 303.00 |
| Thermoform Plastic | $ 6.00 |
| Subtotal | $ 801.00 |

Bibliography

[1] Sing, D., 2012, "Torue Steer Response of Wheeled Single-Track Vehicles," Terre Haute.

[2] Indiana Legislature, 2010, "Indiana Code, Title 9, Article 21, Chapter 11," , O.oC. Revision, ed., Indiana Legislative Services Agency.

[3] Maps.com, 2011, "Average Temperature Map (January),".

[4] Maps.com, 2011, "Average Temperature Map (July),".

[5] Rose-Hulman Human Powered Vehicle Team, 2011, "2011 ASME East Coast HPV Challenge," Rose-Hulman Institute of Technology, Terre Haute, IN.

[6] Crisostomo, C., 2012, "4 Reasons Why Supercapacitors Will Eventually Go Mainstream,".

[7] Cellergy, 2010, "Supercapacitors," Cellergy, Bend, OR.

[8] Cap-XX, 2008, "FAQ," CAP-XX Ltd, Lane Cove, NSW, Australia.

[9] Rose-Hulman Human Powered Vehicle Team, 2010, "Rose-Hulman Institute of Technology 2010 ASME East Coast HPV Challenge," Rose-Hulman Institute of Technology, Terre Haute, IN.

[10] Rose-Hulman Human Powered Vehicle Team, 2009, "2009 Human Powered Vehicle Team Design Report- West," Terre Haute.

[11] National Climatic Data Center, 2004, "Climatography of The United States No. 20".

[12] Brown, S., 2012, "Bicycle Cranks," Harris Cyclery, West Newton, MA.

[13] Owers, D., 1985, "Development of a Human-Powered Racing Hydrofoil," Human Power, **3**(3), p. 13.

[14] Thompson DC, R.FTR., 2009, "Helmets for preventing head and facial injuries in bicyclists (review),".